An accurate method for leakage inductance calculation of shell-type multi core-segment transformers with circular windings

IEEE Access
Multidisciplinary ⋮ Rapid Review ⋮ Open Access Journal

Received June 28, 2021, accepted August 2, 2021, date of publication August 9, 2021, date of current version August 16, 2021.

Digital Object Identifier 10.1109/ACCESS.2021.3103541

An Accurate Method for Leakage Inductance Calculation of Shell-Type Multi Core-Segment Transformers With Circular Windings

MORTEZA ESLAMIAN[1], MOHAMMAD KHAREZY[2], (Member, IEEE), AND TORBJÖRN THIRINGER[3], (Senior Member, IEEE)

[1]Department of Electrical Engineering, University of Zanjan, Zanjan 45371-38791, Iran
[2]Department of High Voltage Measurement Technology, RISE Research Institutes of Sweden, 504 62 Borås, Sweden
[3]Department of Electrical Engineering, Chalmers University of Technology, 412 96 Gothenburg, Sweden

Corresponding author: Morteza Eslamian (eslamian@znu.ac.ir)

This work was supported in part by Swedish Energy Agency, in part by Chalmers, and in part by Research Institutes of Sweden (RISE).

ABSTRACT The leakage field in shell-type transformers is strongly affected by the boundary conditions introduced by the core walls and thus the effect of the core should be considered properly in the leakage inductance calculation. In this paper, a new method for accurate calculation of the leakage inductance of shell-type multi core-segment transformers with circular windings is presented. For this purpose, first, the expressions for self and mutual inductances are derived in cylindrical coordinates considering the core walls as the flux-normal boundary condition. Then, a new approach is proposed for calculating the leakage inductance considering the number and dimensions of the used core segments. The method is developed at first for single and double core-segment transformers (known also as E-core and U-core transformers) and then adopted for shell-type segmented-core transformers. The method is verified by 3-D FEM simulations. The comparisons with the previous analytical methods demonstrate the superiority of the proposed method. A transformer prototype has been built and verification tests have been conducted. The comparisons show that the leakage inductance can be estimated with an error less than 1%, demonstrating a very high accuracy with the proposed method.

INDEX TERMS Leakage inductance, shell-type transformer, Medium Frequency Transformer, MFT.

I. INTRODUCTION

High-power DC-DC converters are gaining interest in applications such as traction and offshore wind farms [1], [2]. A promising candidate for these applications is the Dual Active Bridge (DAB) which apart from the power electronic switches also comprises a Medium Frequency Transformer (MFT). In order to achieve desirable soft-switching characteristics, a minimum series inductance is needed which is integrated in the MFT [3], [4]. Therefore, on the one hand, the MFT is responsible for changing the voltage level and on the other hand, it provides the series inductance required for the switching performance. The value of the MFT's leakage inductance is of great importance for the correct operation of a DAB converter. The converter's efficiency is strongly dependent on the value of the leakage inductance [5].

The associate editor coordinating the review of this manuscript and approving it for publication was Yilun Shang.

The shell-type segmented-core MFTs are suitable alternatives which can be used in high power and high voltage applications with significantly higher rating compared to transformers used in conventional DAB converters. For a constant power, the dimensions of the MFT become smaller by increasing the frequency due to the reduction of the core dimensions as a result of the reduction of the core flux. The use of a high-power MFT implies a high current flow through the transformer windings. This requires a more efficient cooling system which in turn imposes a limitation in reducing the transformer size. Also, in parallel-input series-output DC-DC converters in all-DC offshore wind farms [6], there is a high DC offset voltage between the primary and secondary windings inside MFT. This requires an appropriate insulation system which enforces further restrictions on reducing the distances between windings which is extensively investigated by the authors in their previously reported activity [7]. Recent studies show that, from a practical point of view, for achieving

a certain power and specific voltage conditions in a high-power MFT, there is a specific range for the optimal operating frequency which is 6-20 kHz [8]–[10].

The behavior of the leakage inductance with respect to frequency in high frequency transformers (HFT) is studied up to 2 MHz in [5], [11]–[13], using Dowell method [14] or its improved form [15]. For high-power MFTs with rated frequencies less than 20 kHz, if Litz wire is used, the change of leakage inductance due to the frequency variation is almost negligible [16].

Different analytical methods have been used for the leakage inductance calculation in literature. In the classical approach (which can be found in [17]–[19]), it is assumed that the leakage flux inside windings and in gaps between windings is completely axial while the effect of the radial leakage flux is considered by applying the Rogowski factor to the average height of the windings to obtain a higher equivalent winding's height [18]. The simulations performed in this paper show that although the classical approach is suitable for calculating the leakage inductance of conventional power transformers, it may be inaccurate in the case of shell-type MFTs. In [20], the superposition of the axial and radial components of the leakage field is used to reduce large errors of the classical method.

The leakage inductance calculation using the double Fourier series extension of the leakage field is developed in [21]. The method is originally proposed for the first time by Roth in [22]. Further applications of the Roth's method can be found in [23]–[25] and [26] for the calculation of the leakage inductance per unit length in 2-D planar coordinates.

The method of images with an analytical 2-D solution of the magnetic vector potential is used for the calculation of leakage inductance in [27]. It is also concluded that the classical approach can lead to a considerable error when the windings have unequal heights. The method of images based on an expression of the magnetic vector potential for a rectangular conductor is also used in [28] for the computation of the static leakage inductance of HF transformers. The leakage inductance of toroidal transformers using the classical approach is presented in [29]. A review of the analytical methods of transformer's leakage inductance calculation is also presented in [30].

The Finite Element Method (FEM) has been extensively used for the leakage inductance calculation in literature [31]–[33]. The FEM formulation is independent of the geometrical details and thus it is more accurate than the analytical methods however, it takes substantially more time to evaluate. In addition, a FEM software or a specifically developed FEM program is also needed.

In the previously published article [16], the authors focused on the leakage inductance calculation of shell-type MFTs with rectangular windings. The leakage inductance per unit length is calculated by a double Fourier series analysis in 2-D planar coordinates. A new method for determination of Mean Length of Turns (MLT) considering the distribution of Ampere-turns inside individual layers of the windings is also presented. The current article presents an accurate procedure for the leakage inductance calculation of shell-type MFTs with circular windings.

In 1956 Rabins proposed an analytical method for calculating the power transformer's leakage inductance in cylindrical coordinates [34]. In this method, the windings are assumed to be completely surrounded by the top and bottom yokes and also the core window is assumed to be endless from its outer side as it is the case for large power transformers. Unlike Rabins method, in the new analysis developed in this paper, the core window is assumed to be bounded to the core wall from outside that is for considering the effect of the core's return leg on the leakage inductance of a shell-type transformer. Thus, as a result of differences in geometry and boundary conditions, the expressions derived for the vector potential and the mutual inductances in sections II and III are different from those presented in [34]. The main contribution of the paper is an effective method, based on the leakage inductance relation derived in section III, for calculating the leakage inductance of shell-type transformers with circular windings considering the number and dimensions of the core segments, that is the subject of sections V and VI. By using the presented analytical method, time-consuming FEM simulations can be avoided in the design stage, although in order to verify the accuracy of the proposed method, the results of the 3-D FEM simulations have been presented for a case study. An additional contribution is that experiments have been performed on a MFT prototype and the results have been compared with the results of the analytical methods and FEM. The comparisons show the high accuracy of the presented method for actual high-power MFTs.

II. CALCULATION OF VECTOR POTENTIAL

The axisymmetric geometry used for field analysis in cylindrical coordinates is shown in Fig. 1(a). The solution space is divided into 4 regions as indicated in Fig. 1(b). Radial and axial extensions of all regions are given in Table 1.

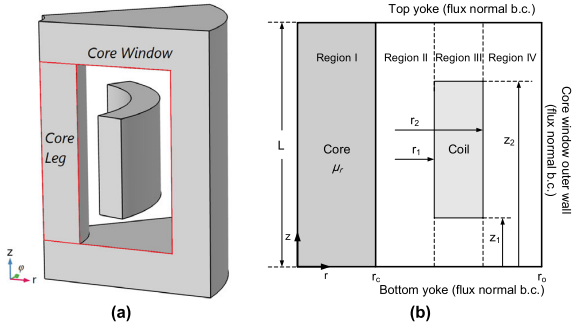

FIGURE 1. (a) The axisymmetric geometry used for field analysis. (b) The geometry divided into solution regions.

The following assumptions are made.

1) The coils are inside the core window and are surrounded by the core walls from all sides.
2) The coils have a rectangular cross section with a uniform current density. The arrangement of the coils is arbitrary.

TABLE 1. Radial and axial extensions of regions in developed method.

Region I	$0 \le r \le r_c$	$0 \le z \le L$
Region II	$r_c \le r \le r_1$	$0 \le z \le L$
Region III	$r_1 \le r \le r_2$	$0 \le z \le L$
Region IV	$r_2 \le r \le r_o$	$0 \le z \le L$

3) The geometry is axisymmetric and the current density vector in the coils is azimuthal.
4) The permeability of the core leg could be of any finite value. Other walls of the core window are defined with the flux-normal boundary condition.

Because of the axisymmetric geometry, all the field quantities are independent of the φ coordinate. The vector potential equation in cylindrical coordinates can be expressed as

$$\frac{\partial^2 A_\phi}{\partial r^2} + \frac{1}{r}\frac{\partial A_\phi}{\partial r} - \frac{A_\phi}{r^2} + \frac{\partial^2 A_\phi}{\partial z^2} = -\mu_0 J_\phi \tag{1}$$

where A_ϕ and J_ϕ are the φ components of the vector potential and current density vector respectively. Note that the subscript φ is dropped for simplicity in the following equations.

The current density could be written as a Fourier series in terms of a fundamental spatial period of length L or window height.

$$J = J_0 + \sum_{n=1}^{\infty} J_n \cos\left(\frac{n\pi z}{L}\right) \tag{2}$$

where J_0 and J_n are the Fourier series coefficients.

Since it's assumed that the yoke material has infinite permeability, the magnetic flux density, $\mathbf{B}$, must be perpendicular to the yoke surfaces. $\mathbf{B}$ is given by

$$\mathbf{B} = \nabla \times \mathbf{A} = -\frac{\partial A}{\partial z} a_r + \frac{1}{r}\frac{\partial (rA)}{\partial r} a_z \tag{3}$$

where a_r and a_z are unit vectors in the r and z directions, respectively. For $\mathbf{B}$ to be perpendicular to the top and bottom yokes, the a_r component of $\mathbf{B}$ must vanish at these yoke positions. If we consider a solution in the form of a series expansion with separated variables as

$$A = \sum_{n=0}^{\infty} R_n(r)\cos(mz), \quad m = \frac{n\pi}{L} \tag{4}$$

then $\partial A/\partial z$ will be zero at $z = 0, L$. Thus, this solution satisfies the flux normal boundary conditions at $z = 0, L$. R_n is a function which only depends on variable r.

Substituting (2) and (4) into (1) and equating corresponding coefficients on both sides of the resulting equation, using the orthogonality of cosine functions, the solution (4) is explicitly obtained as

$$A = Sr + \frac{T}{r} - \frac{\mu_0 J_0 r^2}{3} + \sum_{n=1}^{\infty}\left(C_n I_1(mr) + D_n K_1(mr) - \frac{\pi\mu_0 J_n}{2m^2} L_1(mr)\right) \times \cos(mz) \tag{5}$$

where S, T, C_n, D_n are unknown constants which should be determined using boundary conditions.

In regions I, II and IV the current density is zero and so the terms J_0 and J_n equal zero in these regions. In region I, the T/r term must be dropped since it approaches infinity as $r \to 0$. Also, since $K_1 \to \infty$ as $r \to 0$, D_n must be dropped too. Labeling the solution constants in this region with superscript I, A inside the core becomes

$$A^I = S^I r + \sum_{n=1}^{\infty}\left(C_n^I I_1(mr)\right)\cos(mz) \tag{6}$$

In region II, none of unknown constants in (5) are zero and A becomes

$$A^{II} = S^{II} r + \frac{T^{II}}{r} + \sum_{n=1}^{\infty}\left(C_n^{II} I_1(mr) + D_n^{II} K_1(mr)\right)\cos(mz) \tag{7}$$

In region III, the current density terms must be kept in (5). Also, like region II, none of unknown constants are zero. Thus, the solution in region III is given as

$$A^{III} = S^{III} r + \frac{T^{III}}{r} - \frac{\mu_0 J_0 r^2}{3} + \sum_{n=1}^{\infty}\left(C_n^{III} I_1(mr) + D_n^{III} K_1(mr) - \frac{\pi\mu_0 J_n}{2m^2} L_1(mr)\right) \times \cos(mz) \tag{8}$$

In region IV, the current density is zero and none of unknown constants are zero.

$$A^{IV} = S^{IV} r + \frac{T^{IV}}{r} + \sum_{n=1}^{\infty}\left(C_n^{IV} I_1(mr) + D_n^{IV} K_1(mr)\right)\cos(mz) \tag{9}$$

All region equations already satisfy the boundary conditions at $z = 0, L$. The unknown constants must be determined by satisfying the boundary conditions at $r = r_c, r_1, r_2, r_o$.

The vector potential must be continuous across the interfaces at $r = r_c$, r_1, r_2, otherwise, the $\mathbf{B}$ given will contain infinities. Thus, at $r = r_c$, (6) and (7) must be equal for all z.

$$A^I(r_c) = A^{II}(r_c) \tag{10}$$

Two other similar equations using (7) and (8) and also using (8) and (9) can be written for continuity of A at $r = r_1$ and $r = r_2$ for all z.

In addition to the continuity of A at the interfaces between regions, the tangential component of $\mathbf{H}$ must be continuous across the interfaces. This means that the term B_z/μ_r must be continuous across all interfaces where μ_r is the relative permeability of the core for region I and it is equal to 1 for other regions. Hence, the following additional condition must be satisfied at $r = r_1$ for all z.

$$\frac{1}{\mu_r r}\frac{\partial\left(rA^I\right)}{\partial r} = \frac{1}{r}\frac{\partial\left(rA^{II}\right)}{\partial r} \quad at\ r = r_c \tag{11}$$

TABLE 2. Solution of A inside regions.

Region	Vector Potential (A)	Constants	
I	$A^{I} = S^{I} r + \mu_0 \sum_{n=1}^{\infty} \frac{J_n}{m^2} C_n^{I} I_1(x) \cos(mz)$	$S^{I} = \mu_r S^{II}$	$C_n^{I} = C_n^{II} + D_n^{II} \frac{K_1(x_c)}{I_1(x_c)}$
II	$A^{II} = S^{II} r + \frac{T^{II}}{r} + \mu_0 \sum_{n=1}^{\infty} \frac{J_n}{m^2} \left(C_n^{II} I_1(x) + D_n^{II} K_1(x) \right) \cos(mz)$	$S^{II} = \frac{\mu_0 J_0 (r_2 - r_1)}{2}$ $T^{II} = r_c^2 (\mu_r - 1) S^{II}$	$C_n^{II} = \frac{I_0(x_o) \int_{x_1}^{x_2} tK_1(t)dt + K_0(x_o) \int_{x_1}^{x_2} tI_1(t)dt}{I_0(x_o) - \alpha K_0(x_o)}$ $D_n^{II} = \frac{I_0(x_c) I_1(x_c) (\mu_r - 1)}{I_1(x_c) K_0(x_c) \mu_r + K_1(x_c) I_0(x_c)} C_n^{II} = \alpha C_n^{II}$
III	$A^{III} = S^{III} r + \frac{T^{III}}{r} - \frac{\mu_0 J_0 r^2}{3} + \mu_0 \sum_{n=1}^{\infty} \frac{J_n}{m^2} \left(C_n^{III} I_1(x) + D_n^{III} K_1(x) - \frac{\pi}{2} L_1(x) \right) \cos(mz)$	$S^{III} = \frac{\mu_0 J_0 r_2}{2}$ $T^{III} = T^{II} - \frac{\mu_0 J_0 r_1^3}{6}$	$C_n^{III} = C_n^{II} + \int_0^{x_1} tK_1(t)dt$ $D_n^{III} = D_n^{II} - \int_0^{x_1} tI_1(t)dt$
IV	$A^{IV} = \frac{T^{IV}}{r} + \mu_0 \sum_{n=1}^{\infty} \frac{J_n}{m^2} \left(C_n^{IV} I_1(x) + D_n^{IV} K_1(x) \right) \cos(mz)$	$T^{IV} = T^{III} + \frac{\mu_0 J_0 r_2^3}{6}$	$C_n^{IV} = C_n^{III} - \int_0^{x_2} tK_1(t)dt$ $D_n^{IV} = \frac{I_0(x_o)}{K_0(x_o)} C_n^{IV}$

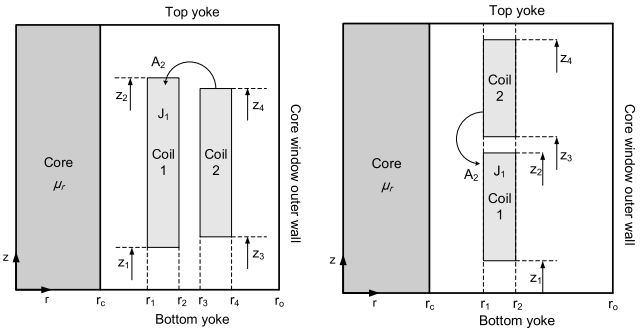

(a) Two radially displaced coils (b) Two axially displaced coils

FIGURE 2. The arrangement of coils inside the core window.

Two other similar conditions can also be written for continuity of H_z at $r = r_1$ and $r = r_2$. Moreover, to satisfy the boundary condition at the outer wall of the core window, the a_z component of **B** must vanish at $r = r_o$ i.e.

$$\frac{\partial \left(rA^{IV} \right)}{\partial r} = 0 \quad at\ r = r_o \tag{12}$$

Solving for the S, T, C_n and D_n constants according to the above conditions and taking out the term $\mu_0 J_n / m^2$ as a common factor from C_n and D_n constants, the solutions in all 4 regions are obtained according to Table 2 where $x_c = mr_c$, $x_1 = mr_1$, $x_2 = mr_2$, $x_o = mr_o$ and $x = mr$.

III. LEAKAGE INDUCTANCE CALCULATION

Using the solution of A inside the core window, self and mutual inductances of a coil system can be obtained. The mutual inductance between coil 1 and coil 2 with currents I_1 and I_2 and uniform current densities J_1 and J_2 is given by

$$L_{12} = \frac{1}{I_1 I_2} \int_{V_1} A_2 J_1 dV_1 \tag{13}$$

When the coils are radially displaced, one can assume that 1 is the inner and 2 is the outer coil (Fig. 2(a)). The result will be independent of this assumption. Substituting for A_2 (region *II* solution for coil 2) and J_1 (Fourier series expansion for current density of coil 1) in (13), after some algebraic operations, the mutual inductance is obtained as

$$\begin{aligned} L_{12,\,drp} &= \frac{\pi r_c^2 \mu_0 (\mu_r - 1) N_1 N_2}{L} + \frac{\pi \mu_0 N_1 N_2}{3L} (r_1^2 + r_1 r_2 + r_2^2) \\ &+ \frac{\pi \mu_0 L}{I_1 I_2} \sum_{n=1}^{\infty} \left\{ \frac{J_{n,1} J_{n,2}}{m^4} \left[C_{n,2}^{II} \int_{x_1}^{x_2} xI_1(x)dx + D_{n,2}^{II} \right. \right. \\ &\left. \left. \int_{x_1}^{x_2} xK_1(x)dx \right] \right\} \end{aligned} \tag{14}$$

where $L_{12,drp}$ is the mutual inductance of two radially displaced coils.

Note that when the coefficients C_n and D_n have a subscript 1, then the expressions given in Table 2 are evaluated using x_1, x_2. However, when the second subscript is 2, then x_3, x_4 must be substituted for x_1, x_2 in the formulas.

If the coils are two coils axially displaced i.e., two coils occupy the same radial position (Fig. 2(b)) then A_2 is the solution of region *III*. In this case, the mutual inductance is

given by

$$L_{12,\,srp} = \frac{\pi r_c^2 \mu_0(\mu_r - 1)N_1N_2}{L} + \frac{\pi\mu_0 N_1N_2}{6L}\left[(r_1+r_2)^2 + 2r_1^2\right] + \frac{\pi\mu_0 L}{I_1I_2}\sum_{n=1}^{\infty}\left\{\frac{J_{n,1}J_{n,2}}{m^4}\left[C_{n,1}^{III}\int_{x_1}^{x_2} xI_1(x)dx + D_{n,1}^{III} \times \int_{x_1}^{x_2} xK_1(x)dx - \frac{\pi}{2}\int_{x_1}^{x_2} xL_1(x)dx\right]\right\} \quad (15)$$

where $L_{12,\,srp}$ is the mutual inductance of two axially displaced coils. It should be noted that the self-inductance of a coil can also be calculated from (15) as the mutual inductance of two coils with the same coordinates.

Now consider N coils (with zero net Ampere-turns) with different dimensions and arbitrary arrangement inside the core window. The leakage inductance can be calculated using the total magnetic energy stored inside the core window. The magnetic energy stored in the system is obtained by

$$W_m = \frac{1}{2}\sum_{i=1}^{N}\sum_{j=1}^{N} L_{ij}I_iI_j \quad (16)$$

where L_{ij} is the mutual inductance of coils i and j, calculated using (14) or (15) depending on the coil arrangement.

Once the total energy is obtained, the leakage inductance can be calculated as

$$L_{leakage} = \frac{2\,W_m}{I^2} \quad (17)$$

where I denotes the current in the side from which the leakage inductance is calculated.

Since for the leakage inductance, the positive and negative Ampere-turns balance exactly, the terms related to the first term of inductances i.e., $\pi r_c^2\mu_0(\mu_r - 1)N_1N_2/L$ in (14) and (15) vanish in the total energy expression. Thus, this term can be dropped from the inductance relations when calculating the leakage inductance, and as a result of this fact, μ_r can also be taken as infinite (without having terms with infinite values in the energy equation), representing a flux normal boundary condition on the inner wall of the core window as well as the flux normal boundary condition on the other sides of the core window. It is noted that as $\mu_r \to \infty$ the parameter α in Table 2 approaches to $I_0(x_c)/K_0(x_c)$ that makes the constants of the solution simpler to evaluate.

The modified Bessel functions generally are available in mathematical computer libraries. Numerical techniques for calculation of the integrals appeared in the formulas (14) and (15) are given in the appendix.

IV. DETERMINATION OF MEAN LENGTH OF TURNS (MLT)

The mean length of turns (MLT) is of great importance in the determination of the leakage inductance for planar windings since the total leakage inductance is obtained by multiplying the leakage inductance per unit length by MLT [16]. According to the relations derived in the previous section, there is no need to scale the calculated leakage inductance since the self and mutual inductances are calculated in H rather than H/m in cylindrical coordinates. Therefore, MLT is not essentially required for the leakage inductance calculation in cylindrical coordinates. However, in order to find the portion of the windings which is surrounded by the core segments, a method for determination of MLT in cylindrical coordinates is developed in this section. The method is similar to the one presented by the authors in [16] but it is adopted for circular windings. The method is based on the total energy stored in the axial leakage field.

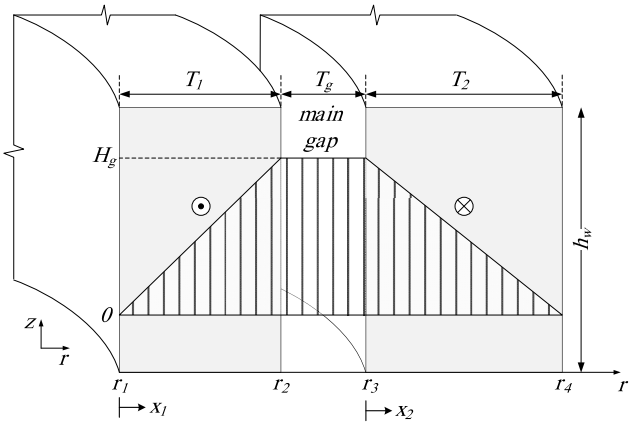

FIGURE 3. Distribution of leakage field inside windings.

According to Fig. 3, the widths of the windings are different in general. The height of both windings is equal to h_w. The net Ampere-turns is zero and the leakage flux outside the windings is neglected. Ampere's law is implemented for calculation of the magnetic field intensity inside the windings. The distribution of magnetic field intensity, H, inside the windings is illustrated in Fig. 3. The field intensity is constant inside the main gap while it changes linearly inside the windings

$$H_g = \frac{NI}{h_w} \quad (18)$$

$$H_1(x_1) = \frac{x_1}{T_1}H_g \quad (19)$$

$$H_2(x_2) = \left(1 - \frac{x_2}{T_2}\right)H_g \quad (20)$$

where NI is the absolute value of the Ampere-turns of each winding. T_1 and T_2 are the widths of windings 1 and 2 respectively. The coordinate parameters x_1 and x_2 are indicated in Fig. 3.

The field strength is constant in the main gap and thus the stored energy in the main gap is given by

$$W_g = \int_{r_2}^{r_3}\frac{1}{2}\mu_0 H_g^2 h_w 2\pi r dr = \frac{1}{2}\pi\mu_0 H_g^2 h_w (r_2 + r_3)\,T_g \quad (21)$$

where T_g is the size of the main gap and r_2 and r_3 are the outer and inner radiuses of windings 1 and 2, respectively.

The inner radius of winding 1 is r_1 and the outer radius of the winding 2 is r_4.

The stored energy in each winding is obtained as the volumetric integral of the magnetic energy density in cylindrical coordinates.

$$W_i = \int_0^{T_i} \frac{1}{2}\mu_0 H_i^2\,(x_i)\,h_w 2\pi\,(r_i + x_i)\,dx_i, \quad i = 1, 2 \tag{22}$$

According to (22), the magnetic energy stored in windings 1 and 2 is individually obtained as

$$W_1 = \frac{1}{2}\pi\mu_0 H_g^2 h_w \left(\frac{1}{3}\left(2r_1 + \frac{3}{2}T_1\right)T_1\right) \tag{23}$$

$$W_2 = \frac{1}{2}\pi\mu_0 H_g^2 h_w \left(\frac{1}{3}\left(2r_2 + \frac{1}{2}T_2\right)T_2\right) \tag{24}$$

Now consider Fig. 4. Each winding is substituted with an equivalent gap with a constant field intensity equal to H_g and an equivalent infinitely thin winding with the same Ampere-turns as before. H_g is the value of the field intensity in the main gap. The width of each equivalent gap is determined in such a way that the stored energy in the equivalent gap is equal to the energy stored inside the corresponding winding.

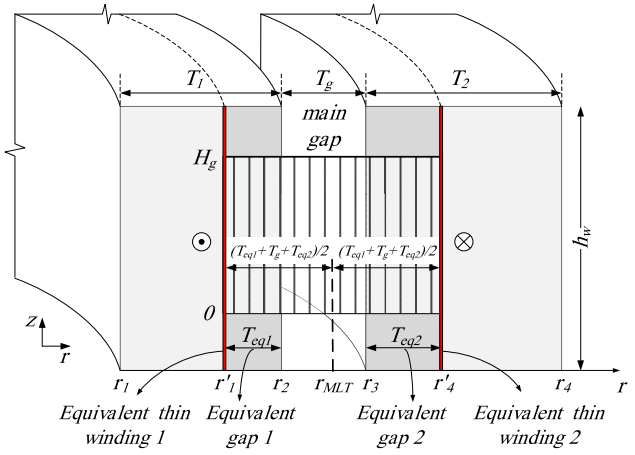

FIGURE 4. The windings are substituted with equivalent thin windings and equivalent gaps to create a gap with a uniform field intensity equal to the field intensity of the main gap and with an energy equal to the total energy of the leakage field.

According to Fig. 4, the energies stored in the equivalent gaps are given by

$$W_1 = \frac{1}{2}\pi\mu_0 H_g^2 h_w \left(r_2^2 - r_1'^2\right) \tag{25}$$

$$W_2 = \frac{1}{2}\pi\mu_0 H_g^2 h_w \left(r_4'^2 - r_3^2\right) \tag{26}$$

Equating (25) with (23) and (26) with (24), r'_1 and r'_4 are obtained as

$$r'_1 = \sqrt{r_2^2 - \frac{1}{3}\left(2r_1 + \frac{3}{2}T_1\right)T_1} \tag{27}$$

$$r'_4 = \sqrt{r_3^2 + \frac{1}{3}\left(2r_2 + \frac{1}{2}T_2\right)T_2} \tag{28}$$

Knowing r'_1 and r'_4, the radius of MLT, r_{MLT}, can be determined as

$$r_{MLT} = \frac{r'_1 + r'_4}{2} \tag{29}$$

Once r_{MLT} is determined, the total stored energy i.e., the energy stored inside the windings and the main gap, can also be calculated as

$$W_T = \frac{1}{2}\mu_0 H_g^2 h_w\,(2\pi\, r_{MLT})\left(T_{eq1} + T_g + T_{eq2}\right) \tag{30}$$

where T_{eq1} and T_{eq2} are the widths of the equivalent gaps of windings 1 and 2, respectively.

In most cases, r_{MLT} is close to the average radius $r_m = (r_1 + r_4)/2$. However, as the difference in the widths of the windings increases, r_{MLT} deviates from r_m, resulting in a MLT different from the one conventionally used that is a circular path in the middle of the total width of the windings and the main gap.

The method presented in this section can be developed for the cases where each winding needs to be modeled layer-by-layer. The method has been discussed in [16] for planar windings which can be extended for axisymmetric windings considering the approach provided in this section.

Using the total energy stored in the axial leakage field, W_T, it is possible to derive a relation for the leakage inductance similar to the relations presented in literature for conventional power transformers [17]. The leakage inductance considering the radial component of the leakage field using the Rogowski factor is given by

$$L_{leakage,classical} = k_r \frac{2\,W_T}{I^2} \tag{31}$$

where W_T is obtained from (30) and I is the current of the excited winding. The Rogowski factor, k_r, is obtained as [17]

$$k_r = 1 - \frac{1 - e^{-\frac{\pi h_w}{(T_1+T_g+T_2)}}}{\pi h_w/(T_1 + T_g + T_2)} \tag{32}$$

In (32), h_w is the average height of the windings and is calculated as $(h_{w1} + h_{w2})/2$ where h_{w1} and h_{w2} are the heights of windings 1 and 2, respectively.

The leakage inductance calculated according to (31) is referred to as the leakage inductance calculated by the classical method in the remainder of the paper.

V. SHELL-TYPE SINGLE AND DOUBLE CORE-SEGMENT TRANSFORMERS

The shell-type single and double core-segment transformers, known also as U-core and E-core transformers are shown in Fig. 5(a) and (b), respectively. Top views of the transformers are shown in Figs. 6 and 7. As can be seen, some parts of the windings are surrounded by the core, resulting in a rise in the leakage inductance value. According to Fig. 6, the corresponding angle of the part of MLT which is surrounded by the core is obtained as follows.

$$\theta = 2\arcsin\left(\frac{a/2}{r_{MLT}}\right) \tag{33}$$

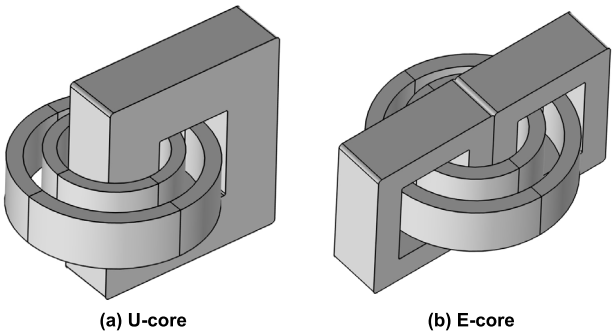

(a) U-core (b) E-core

FIGURE 5. Shell-type single and double core-segment transformers.

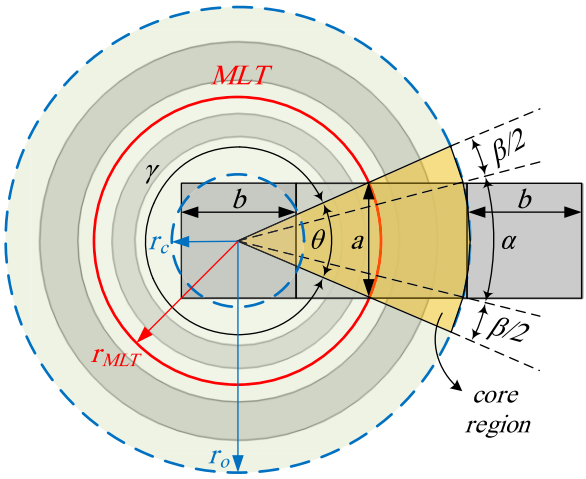

FIGURE 6. A top view of a shell-type single core-segment transformer.

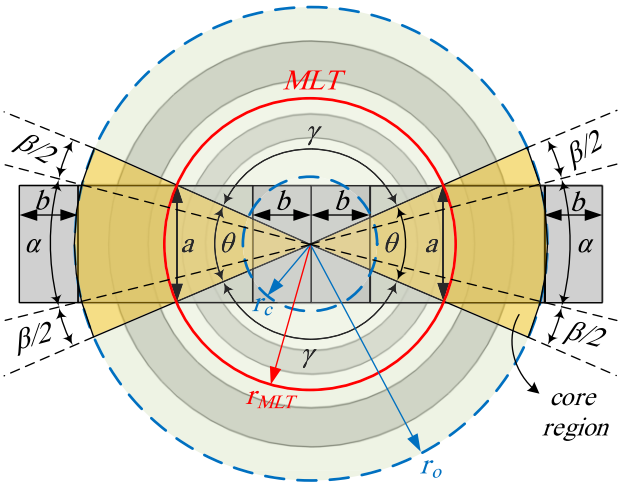

FIGURE 7. A top view of a shell-type double core-segment transformer.

where a is the thickness of the core segment and θ is the angle of the core region wherein the windings are surrounded by the core yokes at top and bottom.

The angle of θ can be considered as the summation of the two angles α and β. For α, the windings are adjacent to

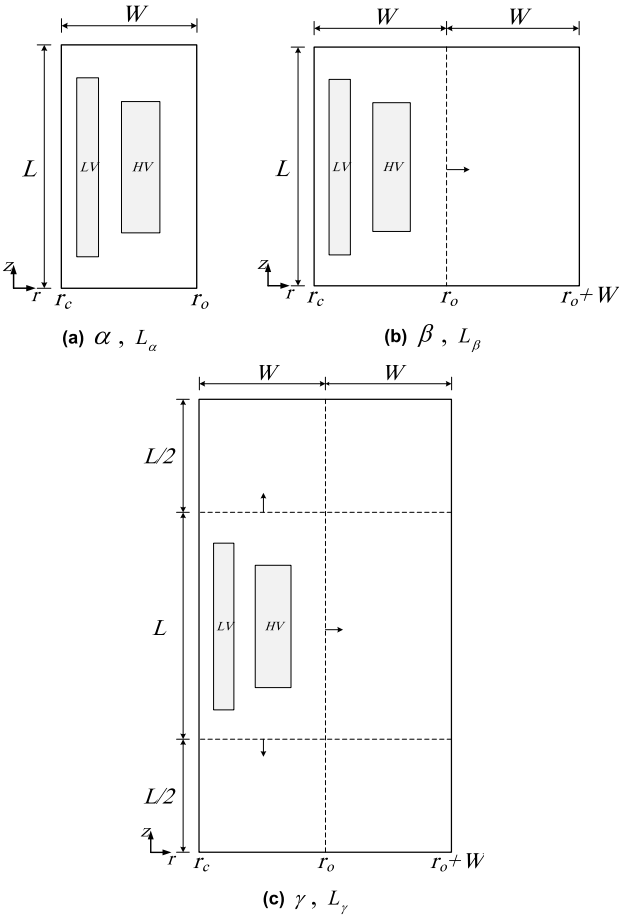

FIGURE 8. Core window arrangements and the relevant angles (in a sector equal to $2\pi/n_c$) and the corresponding leakage inductances for single and double core-segment transformers (a) actual core window (b) core window, unbounded from outside (c) core window, unbounded from outside, with displaced top and bottom core walls used for outside the core region.

the core's return leg in the radial direction. The angle α is calculated as

$$\alpha = 2\arcsin\left(\frac{a/2}{r_o}\right) \tag{34}$$

where r_o is the radius of the inner wall of the core's return leg. In the region equal to the angle of γ (outside the core region) the windings are outside the core window and are not surrounded by the core yokes. According to Fig. 7, for a shell-type E-core transformer, the core has two segments and the windings are surrounded by the core in two regions with the total angle of 2θ. For calculation of the leakage inductances related to the regions with the angles α, β and γ, the core window arrangements shown in Fig. 8 are used.

In the region with the angle of α, the windings are adjacent to the core walls from all sides and therefore, according to Fig. 8(a), the leakage inductance is calculated inside the core window with the actual dimensions. In the region with the angle of β, the windings are not adjacent to the core's return leg from outside. Therefore, according to Fig. 8(b), the outer

wall of the core window is moved away from the windings. For this purpose, the width of the core window has been doubled, which is enough to neutralize the effect of the outer wall of the core window. For the region with the angle of γ, according to Fig. 8(c), in addition to the outer wall of the core window, the top and bottom walls of the core window are moved to a farther distance. As a result of this displacement, the height of the core window is doubled, which is sufficient to eliminate the effect of the core yokes on the leakage field.

If the leakage inductances corresponding to the core window arrangements shown in Figs. 8(a), 8(b) and 8(c) are denoted by L_α, L_β and L_γ respectively, the total leakage inductance is obtained as

$$L_{leakage}^{total} = \frac{n_c}{2\pi}\left(\alpha L_\alpha + \beta L_\beta + \gamma L_\gamma\right) \tag{35}$$

where n_c is the number of the core segments. n_c is equal to 1 for the single core-segment transformer and equal to 2 for the double core-segment transformer. Note that L_α, L_β and L_γ are calculated separately by (17) with the relevant dimensions for the core window.

It should be noted that the equivalent radius of the core, r_c, regarding the criterion of the constant cross-sectional area of the core, is calculated by

$$r_c = \sqrt{\frac{k}{\pi}(a \times b)}, \quad k = 1, 2 \tag{36}$$

where k is equal to 1 for the single core-segment transformer and 2 for the double core-segment transformer. b is the width of the core leg and core yoke.

VI. SHELL-TYPE SEGMENTED-CORE TRANSFORMERS

The circular windings are preferred over the commonly used rectangular windings in the shell-type MFTs with high isolation requirements for the HV winding. In addition to using circular windings, the core segments can also be distributed along the circumference of the winding region. The distribution of core segments is actually due to reasons such as overcoming the physical constraints, providing the permissible electrical clearances and the maximum use of the available space to create more symmetry in the geometry of the transformer. The leakage inductance of the transformer also increases with the distribution of the core segments. The reason is that the leakage flux is more affected by the core walls as the core segments are distributed, leading to a higher value of the leakage inductance. This necessitates the establishing of a new method, different from the one presented in the previous section, for calculating the leakage inductance of the shell-type transformers with $n_c > 2$ which are referred to as the shell-type segmented-core transformers in this paper.

A top view of a shell-type transformer with a regular polygonal core structure is shown in Fig. 9. As can be seen, only some parts of the windings are surrounded by the core and thus the result of the leakage inductance calculation with the windings entirely situated inside the core window will exceed

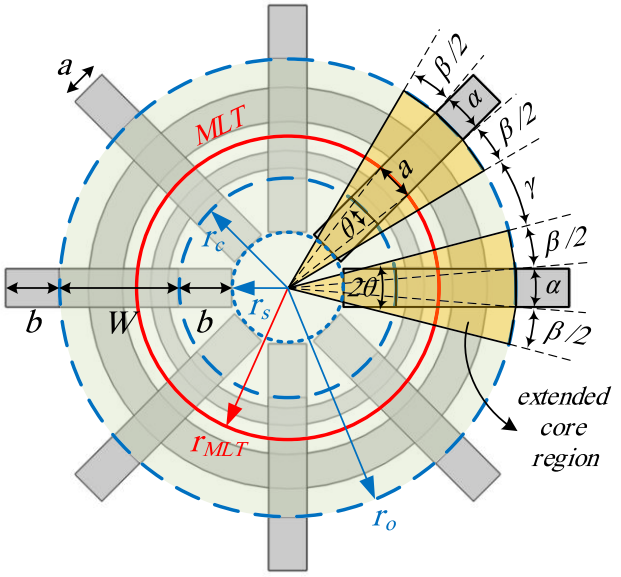

FIGURE 9. A top view of a shell-type Transformer with a regular polygonal core (segmented-core) structure.

the real value. From another point of view, although each core segment geometrically surrounds a relatively small part of the windings, the entire winding region, including the parts which are not surrounded by the core, is magnetically affected by the core. This is essentially due to the high permeability of the core, which causes leakage flux to be absorbed by the core walls between core segments. The vicinity of the core segments reinforces this effect. As a result, the leakage inductance will be underestimated if only those parts of the windings which are geometrically covered by the core segments are assumed to be inside the core window as it was implemented for the single and double core-segment transformers. Therefore, an appropriate method is required for calculating the leakage inductance considering the core effect more accurately. A suitable solution was found by examining the core effect on the leakage flux through extensive investigations of multiple dedicated 3-D FEM simulations. An extended core region is considered around each core segment wherein the windings are strongly influenced by the core and thus it is assumed that the windings are completely surrounded by the top and bottom yokes in this region (brown-colored region in Fig. 9). The equivalent angle of each extended core region is 2θ, which is twice the angle of the core region used for the single and double core-segment transformers. θ is illustrated in Fig. 9 and is calculated by (33).

The middle sector of each extended core region that is equal to an angle of $\alpha \simeq a/r_o$, is bounded by the core's return leg in the radial direction and thus in this region, the windings are adjacent to the outer wall of the core window from outside. In the remaining sectors, equal to an angle of $\beta = \theta - \alpha$ in total, the windings are not near the outer wall of the core window.

According to the regions specified in Fig. 9, the leakage inductance is calculated for three different core window

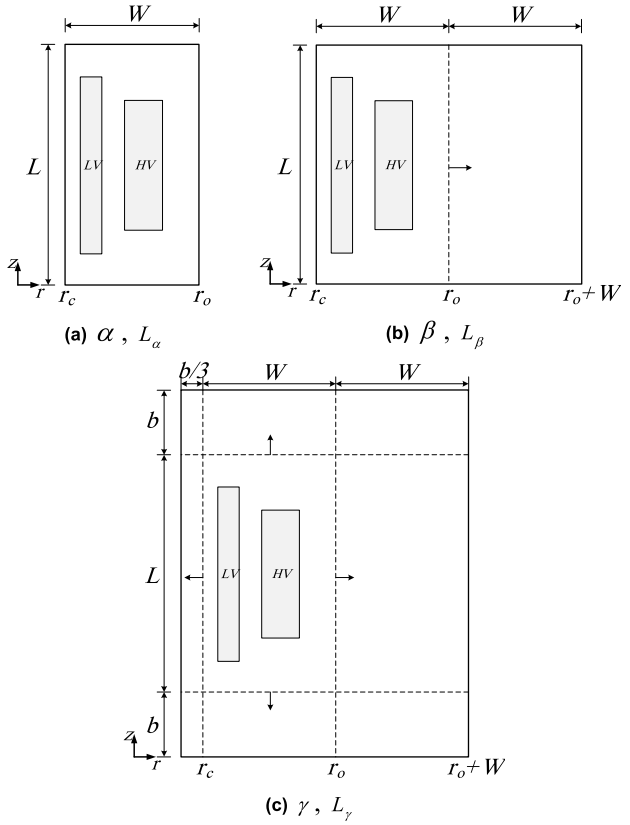

FIGURE 10. Core window arrangements and the relevant angles (in a sector equal to $2\pi/n_c$) and the corresponding leakage inductances for segmented-core transformers (a) actual core window (b) core window, unbounded from outside (c) core window, unbounded from outside, with displaced top and bottom core walls used for the region situated between two extended core regions.

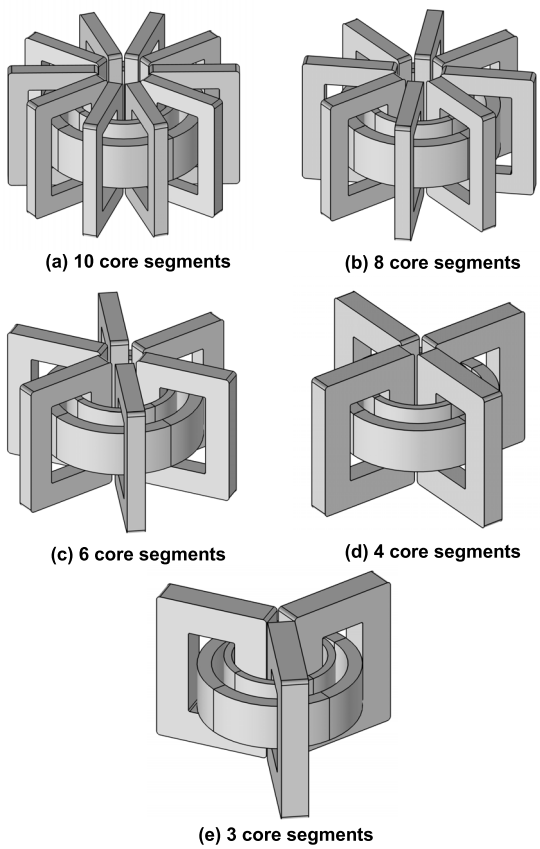

FIGURE 11. A shell-type transformer with different numbers of core segments ($n_c > 2$).

arrangements, as shown in Fig. 10. The total leakage inductance is calculated as a combination of the leakage inductance values obtained for these arrangements. The arrangement shown in Fig. 10(a) is used to calculate the leakage inductance for those parts of the windings which are surrounded by the core and thus situated completely inside the core window (region with the angle of α). To calculate the leakage inductance for those parts of the windings which are not adjacent to the core's return leg (region with the angle of β), the outer wall of the core window is displaced in the radial direction as shown in Fig. 10(b). The amount of the displacement is the same as the width of the core window that is enough to neutralize the effect of the core's outer wall. In the region situated between two adjacent extended core regions (equal to an angle of $\gamma = 2\pi/n_c - \theta$), the effect of the core is lower and thus, the core walls are assumed to be farther than the distance for the extended core region. The suitable displacement of the core walls for this region is demonstrated in Fig. 10(c). Once the leakage inductances corresponding to the core window arrangements shown in Fig. 10 are obtained, the total leakage inductance is obtained by (35).

The method presented in this section is for calculation of the leakage inductance of a shell-type transformer with a regular polygonal core structure. The proposed method can still be used to calculate the leakage inductance of a shell-type transformer with an irregular polygonal core structure. For this purpose, first the transformer with irregular core structure is converted to a transformer with regular core structure with the same number of core segments and then the method is employed to calculate the total leakage inductance. The results of the FEM simulations presented in Section VIII confirm the validity of the procedure.

VII. SENSITIVITY ANALYSIS

In order to verify the proposed method, a sensitivity analysis is performed on a shell type transformer in three cases for different numbers of core segments.

The number of the core segments for $n_c > 2$ is changed in such a way that the flux density inside the core remains constant (see Fig. 11). As the number of the core segments, n_c, is reduced, the total cross-sectional area of the core segments is increased proportionally. This is accomplished by increasing the parameters a and b of the core segments (indicated in Fig. 9) by the same factor and also by a slight reduction in r_c (shown in the same figure) to make it possible to apply the required changes.

For the shell-type transformers with $n_c \leq 2$ i.e., the single and double core-segment transformers, the simulations

TABLE 3. Leakage inductance results from the sensitivity analysis for segmented-core transformers.

		10 core segments			8 core segments			6 core segments			4 core segments			3 core segments		
		Case 1	Case 2	Case 3	Case 1	Case 2	Case 3	Case 1	Case 2	Case 3	Case 1	Case 2	Case 3	Case 1	Case 2	Case 3
Leakage Inductance (μH)	3-D FEM	26.71	31.19	37.56	26.54	30.94	37.22	26.25	30.55	36.69	25.78	29.92	35.83	25.44	29.48	35.22
	Proposed Method	26.67	31.09	37.43	26.47	30.83	37.07	26.21	30.48	36.60	25.83	29.99	35.93	25.61	29.71	35.55
	Rabins Method [34]	27.14	31.91	38.65	27.13	31.90	38.64	27.12	31.89	38.63	27.10	31.88	38.61	27.03	31.82	38.54
	Classical Method (31)	27.90	31.79	38.14	27.90	31.79	38.14	27.90	31.79	38.14	27.90	31.79	38.14	27.90	31.79	38.14
Absolute Relative Error (%)	Proposed Method	0.1	0.3	0.3	0.3	0.4	0.4	0.2	0.2	0.2	0.2	0.2	0.3	0.7	0.8	0.9
	Rabins Method	1.6	2.3	2.9	2.2	3.1	3.8	3.3	4.4	5.3	5.1	6.6	7.8	6.3	7.9	9.4
	Classical Method	4.5	1.9	1.5	5.1	2.7	2.5	6.3	4.1	4.0	8.2	6.3	6.4	9.7	7.8	8.3

TABLE 4. Leakage inductance results from the sensitivity analysis for single and double core-segment transformers.

		2 core segments (a=b)			2 core segments (a=2b)			1 core segment (a=b/2)			1 core segment (a=b)		
		Case 1	Case 2	Case 3	Case 1	Case 2	Case 3	Case 1	Case 2	Case 3	Case 1	Case 2	Case 3
Leakage Inductance (μH)	3-D FEM	24.99	28.90	34.44	25.25	29.25	34.93	24.57	28.29	33.61	24.63	28.38	33.74
	Proposed Method	24.85	28.73	34.23	25.06	29.01	34.61	24.58	28.38	33.77	24.69	28.52	33.96
	2-D planar method [22]	25.14	28.20	33.63	25.35	28.48	34.00	24.86	27.84	33.15	24.97	27.97	33.34
Absolute Relative Error (%)	Proposed Method	0.6	0.6	0.6	0.8	0.8	0.9	0.0	0.3	0.5	0.2	0.5	0.7
	2-D planar method	0.6	2.4	2.4	0.4	2.6	2.7	1.2	1.6	1.4	1.4	1.4	1.2

The error's background color: white for smaller than 1 %, yellow for 1 to 2 %, orange for 2 to 3 % and red for larger than 3 %.
Case 1: The dimensions of the windings are the same as the fabricated prototype's.
Case 2: The LV winding's radial width is increased by 9 mm.
Case 3: The LV winding's radial width is increased by 9 mm and the main gap is also increased by 6 mm.

are performed for two different ratios of a and b (indicated in Figs. 6 and 7) whereas the total cross-sectional area of the core is still kept constant.

For case 1, the dimensions of the windings are equal to the dimensions of the windings of the transformer prototype under study in this paper. For case 2, the radial width of the LV winding is increased by 9 mm representing an addition of three cooling ducts, each with a width of 3 mm, between the LV layers, considering a uniform Ampere-turns model of the LV winding. As a result of increasing the LV width, the HV winding's inner diameter is increased accordingly, to keep the main gap between the windings constant. The width of the core window is also increased proportionally to keep the HV winding's distance to the outer wall of the core window constant. For case 3, in addition to an increase in the LV winding's width equal to 9 mm, the width of the main gap is also increased by 6 mm to provide more clearances between the LV and HV windings. Similar to case 2, as a result of increasing the inner diameter of the HV winding, the width of the core window is also increased accordingly to preserve the distance between the HV winding and the outer wall of the core window. In both cases 2 and 3, the height of the windings, the height of the core window, the inner diameter of the LV winding and the width of the HV winding remain constant.

The results of the leakage inductance calculation using the proposed method and using the 3-D FEM as the reference method are shown in Table 3 for $n_c > 2$. The accuracy of the proposed method is also compared with Rabins method [34] as well as the classical method. Equation (31) is used for the calculation of the leakage inductance according to the classical method. According to Table 3, the accuracy of the proposed method in all cases for different numbers of core segments is higher than the accuracy of the other methods (less than 1 % in all cases). It should be noted that although the parameter θ is dependent on the dimensions of the core segments, the accuracy of the proposed method is independent of the value of this parameter. It can be seen from Table 3 that the error of Rabins method increases especially as the number of the core segments decreases. Note that the number and dimensions of the core segments are not properly reflected in the geometry in Rabins method, leading to inaccurate results in the leakage inductance calculation. According to Table 3, the classical method produces inaccurate results in all cases. It should be noted that the core walls do not affect the value of leakage inductance in the classical method.

The results of the leakage inductance calculation for the single and double core-segment transformers are shown in Table 4. The error of the proposed method in comparison with the 3-D FEM is less than 1% in all cases. Rabins as well as the classical methods are not suitable to apply for the single and double core-segment transformers (due to large errors) and thus their results are not presented in Table 4. The results of the leakage inductance calculation using the 2-D planar method is also provided in Table 4. In the 2-D planar method, the leakage inductance per unit length is calculated based on a double Fourier series expansion of the field quantities in the cartesian coordinates [21], [22]. The total leakage

inductance is then obtained by multiplying the inductance per unit length by the mean length of turns (*MLT*). The middle of the total width including the widths of the windings and the main gap is used to determine the *MLT*. In this regard, the *MLT* is the perimeter of a hypothetical circle having a diameter equal to the average of the inner diameter of the LV winding and the outer diameter of the HV winding. Based on the part of the *MLT* which is surrounded by the core segments, the *MLT* is divided in two partial lengths MLT_{in} and MLT_{out} [26]. If the leakage inductances per unit length calculated inside and outside the core window are referred to as l_{in} and l_{out} respectively, the total leakage inductance is obtained by the summation of $MLT_{in}l_{in}+MLT_{out}l_{out}$. l_{in} is calculated using Roth's method. l_{out} is also calculated using Roth's method but by moving the core walls far enough away from the windings. The formulation of the Roth's method is extensively described in [16]. The core window arrangements used for calculation of the leakage inductances inside and outside the core window are the ones shown in Fig. 8(a) and Fig. 8(c), respectively.

The results of the 2-D planar method presented in Table 4 show that neglecting the curvature of the windings may lead to errors of more than 2.5% in some cases. Note that in the 2-D planar method the windings are no longer regarded as cylindrical rings but as parallel bars of infinite length. This approves the advantage of using an axisymmetric analysis for an accurate estimation of the leakage inductance of a transformer with circular windings. It should be noted that the 2-D planar method is not appropriate to be applied on the shell-type transformers with $n_c > 2$ due to the complexity of the boundary conditions for those parts of the windings which are located outside the core window and thus the 2-D planar method is not included in Table 3.

Regarding the computation time required for the calculations, it is worth mentioning that the proposed method and the 2-D planar method are not much different in view of the calculation cost. The relation (35) can be evaluated within about 90 ms (30 ms for each core window arrangement), with 50 components to assess the infinite series of the inductance relations mathematically using the programming platform of MATLAB. The Rabins method takes one third of this time with the same number of the components. The 2-D planar method takes nearly the same time needed by the proposed method (about 80 ms) where 50 components are used for each of the x and y variables to evaluate the double infinite series. An equivalent 3-D FEM simulation in the same PC used for the proposed method takes nearly 10 minutes to solve. The implementation of the classical method is much simpler, but it is inaccurate in the case of the MFT studied in this article. It should be noted that the computation time is essentially a function of the specifications of the computer system used and may vary from one system to another. Therefore, it is possible to achieve less computation times using a higher performing computer system and also by implementing more efficient programming techniques.

The 3-D FEM is very accurate, however, in many cases several simulations need to be run to study various design variants of a transformer, resulting in a considerable solution time while the analytical method is several thousand times quicker, making it possible to have a much more advanced optimization with a shorter total time. A possibility is to use 2-D magnetostatic FEM, however, at the cost of much longer calculation time compared to the analytical model.

VIII. FEM SIMULATION

COMSOL Multiphysics is used for 3-D FEM analysis of the leakage field inside the MFT under study in this paper. The windings are modeled as stranded coils with uniform current densities. The net Ampere-turns of the windings is equal to zero to represent the short-circuit test condition used for the leakage inductance measurement. The core is modeled as a linear magnetic material with high relative permeability. The windings and surrounding medium are specified as non-magnetic materials with a relative permeability equal to 1. The electrical conductivity is defined zero for all materials. A stationary study is used. The outer surface of the domain is defined as the magnetic insulation (flux-parallel boundary condition).

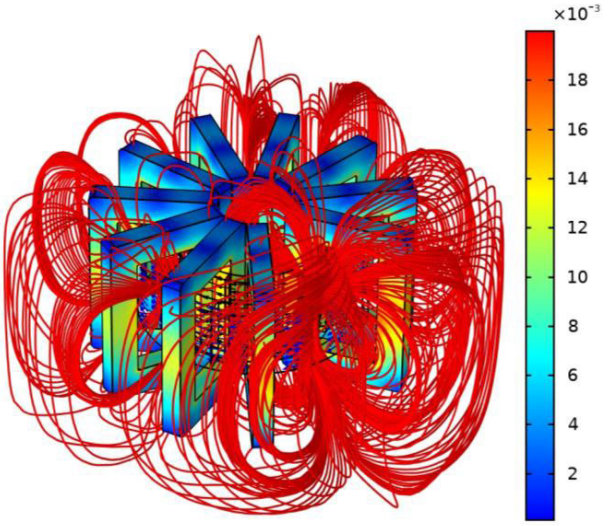

FIGURE 12. The leakage field obtained by 3-D FEM simulation (T).

The result of the leakage field analysis using 3-D FEM is displayed in Fig. 12. The distribution of the leakage flux density inside the core window is also shown in Fig. 13. It is noted that the low value of the flux inside the core is due to the condition of the zero-net Ampere-turns of the windings. As can be deduced from Figs. 12 and 13, the core changes the shape of the leakage flux, affecting the leakage inductance consequently. This implies the necessity of using more accurate analytical methods since the classical leakage inductance formulas may not be accurate enough in this case.

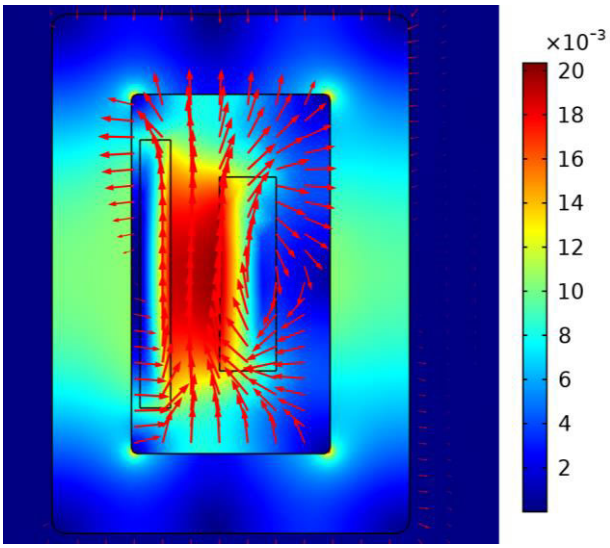

FIGURE 13. Distribution of leakage flux density (T) inside the core window.

The leakage inductance calculated using 3-D FEM is 26.65 μH. The leakage inductance is calculated using the total magnetic energy stored in the leakage field which is the energy stored outside the core segments. The leakage inductance calculated by the proposed method is 26.67 μH. The difference between the proposed method and FEM is less than 0.1%, demonstrating an excellent accuracy for the proposed method for the leakage inductance calculation of shell-type transformers with circular windings.

IX. TEST OBJECT AND EXPERIMENTAL VERIFICATION

A 50 kW, 421.9/4500 V, 5 kHz, oil-type MFT is designed and fabricated with a high DC voltage insulation withstand on the high voltage winding against the low voltage winding and the core walls. The prototype is shown in Fig. 14 including the MFT active part, Plexiglas tank and insulation oil circulation and cooling system. The high frequency content of the voltage waveform applied to the MFT windings dictates the use of a magnetic core with low AC losses at high frequencies. A set of 10 Ferrite magnetic cores are used for this purpose. A Litz wire with dimensions of 3.8 mm × 2.5 mm is used for the production of the windings.

A composite oil-solid insulation system is used as an effective solution for the isolation requirements. The pressboard barriers are used to subdivide the oil ducts into smaller ones, as can be seen from Fig. 15. The HV winding height is kept shorter than the LV winding height because the stress at the LV corners facing the HV winding is lower in this case. Reducing the HV winding height is also done in order to keep the HV winding far from the core edges at the top and bottom. To minimize high electric stresses at the winding's sharp edges, the commonly used rectangular-shaped windings [7] are replaced with circular windings which are more suitable for MFTs with high voltage applications. As a result of using circular windings, the core segments are also distributed

FIGURE 14. The MFT prototype used as the test object.

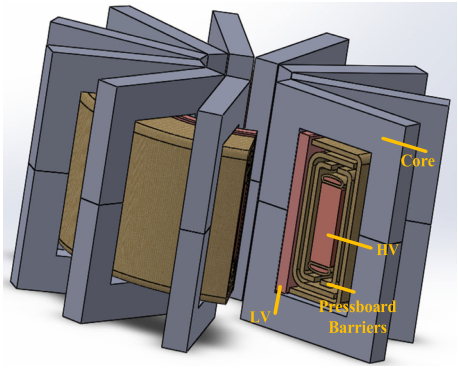

FIGURE 15. A cross view of internal insulation of the fabricated MFT.

along the circumference of the winding region. To prevent the occurrence of breakdown between the high voltage leads and the grounded core walls, due to the strong electric fields, no core segment is considered near the place where the leads are taken out. Due to the isolation requirements of the high voltage winding, the dimensions of the windings and the clearances inside the core window undergo unavoidable changes, which affect the leakage inductance of the windings accordingly. In fact, increasing the gap between the windings and increasing the difference in heights of the windings give rise to the leakage flux and the leakage inductance consequently. Considering the importance of the leakage inductance value of a MFT in optimal operation of a DC-DC converter, there may be a compromise between achieving the optimum insulation design and reaching the desired leakage inductance in practice. This makes the design of MFTs with high DC offset voltage on their HV winding a rather complex task.

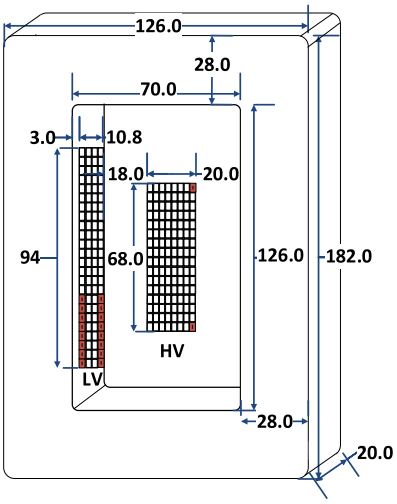

FIGURE 16. The dimensions of the MFT used as test object in mm ($r_s = 36$ mm).

The dimensions of the MFT prototype are indicated in Fig. 16. The LV winding has 12 turns and it is wound in four layers. Due to the high current of the LV winding and regarding the highest allowable current of a Litz wire, 8 parallel wires are used for each turn in the axial direction. The secondary winding has 128 turns and it is built in the form of a disc winding. It consists of 16 discs each wound in the radial direction with 8 turns. The rated currents of the LV and HV windings are 118.5 and 11.11 A respectively.

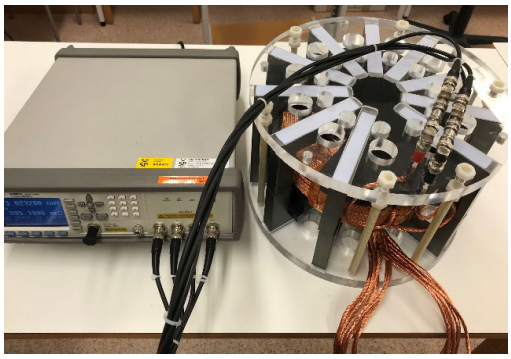

FIGURE 17. The test setup for leakage inductance measurement.

The leakage inductance of the fabricated prototype is measured by an Agilent E4980A RLC meter. The test setup is shown in Fig. 17. The leakage inductance measured from the LV side is presented in Fig. 18. As can be seen, the leakage inductance remains almost constant in the measurement frequency range. This proves the small influence of the eddy current effects on the leakage inductance as a result of using Litz wire in the windings. The measured value for the leakage inductance is 26.46 μH. The result of the 3-D FEM and the proposed method are compared with the measurement in Table 5. The values of relative percent errors for 3-D FEM and the proposed method are both less than 1 percent,

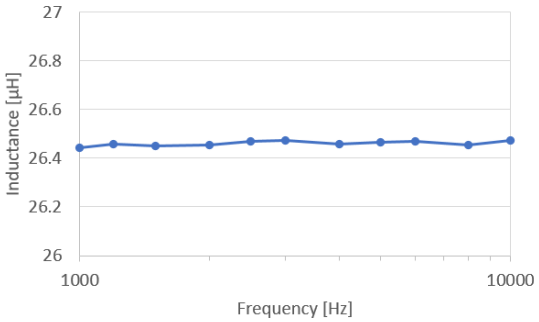

FIGURE 18. The leakage inductance measured as a function of frequency.

TABLE 5. Results of leakage inductance calculation.

Measurement (μH)	3-D FEM (μH)	Proposed Method (μH)	3-D FEM Absolute Error (%)	Proposed Method Absolute Error (%)
26.46	26.65	26.67	0.7	0.8

indicating a small deviation between measured and calculated leakage inductances.

X. CONCLUSION

In this paper, an accurate analytical method for calculating the leakage inductance of shell-type transformers with circular windings is presented. The expression provided for the leakage inductance is based on a field analysis in cylindrical coordinates considering the effect of core walls as the flux-normal boundary condition. The classical method as well as Rabins method suffer from unrealistic assumptions for the core's structure where an accurate estimation of the leakage inductance is vital. The 2-D planar method is not accurate enough due to the neglecting of the curvature of the windings and using the mean length of turns as a scaling factor for the calculated leakage inductance per unit length. The method proposed in this paper enables calculation of the leakage inductance taking the core's structure into account. The comparisons with the results of the 3-D FEM simulations prove the higher accuracy of the proposed method compared with the previously presented analytical approaches.

The proposed method is also applied to a fabricated transformer prototype and the result is experimentally verified. It is confirmed by the measurements that due to the use of Litz wires, the leakage inductance variation is negligible in the frequency range of 1-10 kHz. The comparisons with the results of measurement show that the error of leakage inductance calculation using the proposed method is less than 1%. The accuracy of the proposed method, in contrast to the previously presented ones, is not affected noticeably by the number of the core segments. In this way, several designs can be quickly checked with highest accuracy, without running time-consuming 3-D FEM simulations.

APPENDIX

In order to calculate the integrals involved with the modified Bessel and Struve functions of order 1, the following expressions can be used [35].

$$\int_0^x tI_1(t)dt = \frac{\pi}{2}x\left[M_1(x)I_0(x) - M_0(x)I_1(x)\right] \quad (37)$$

$$\int_0^x tK_1(t)dt = \frac{\pi}{2}\left\{1 - x\left[M_1(x)K_0(x) + M_0(x)K_1(x)\right]\right\} \quad (38)$$

$$\int_0^x tL_1(t)dt = -xM_0(x) - \frac{x^2}{\pi} + \int_0^x M_0(t)dt + \int_0^x tI_1(t)dt \quad (39)$$

where

$$M_0(x) = \frac{2}{\pi}\int_0^{\pi/2} e^{-x\cos\theta}d\theta \quad (40)$$

$$M_1(x) = \frac{2}{\pi}\left(1 - \int_0^{\pi/2} e^{-x\cos\theta}\cos\theta\, d\theta\right) \quad (41)$$

$$\int_0^x M_0(t)dt = \frac{2}{\pi}\int_0^{\pi/2}\frac{\left(1 - e^{-x\cos\theta}\right)}{\cos\theta}d\theta \quad (42)$$

ACKNOWLEDGMENT

The authors would like to thank Karl-Erik Rydler from RISE for his contribution in leakage inductance measurements.

REFERENCES

[1] F. Blaabjerg, M. Liserre, and K. Ma, "Power electronics converters for wind turbine systems," *IEEE Trans. Ind. Appl.*, vol. 48, no. 2, pp. 708–719, Mar./Apr. 2012.
[2] M. Forouzesh, P. Y. Siwakoti, A. S. Gorji, F. Blaabjerg, and B. Lehman, "Step-up DC–DC converters: A comprehensive review of voltage-boosting techniques, topologies, and applications," *IEEE Trans. Power Electron.*, vol. 32, no. 12, pp. 9143–9178, Dec. 2017.
[3] M. A. Bahmani, T. Thiringer, and M. Kharezy, "Design methodology and optimization of a medium-frequency transformer for high-power DC-DC applications," *IEEE Trans. Ind. Appl.*, vol. 52, no. 5, pp. 4225–4233, Sep./Oct. 2016.
[4] B. Chen, X. Liang, and N. Wan, "Design methodology for inductor-integrated litz-wired high-power medium-frequency transformer with the nanocrystalline core material for isolated DC-link stage of solid-state transformer," *IEEE Trans. Power Electron.*, vol. 35, no. 11, pp. 11557–11573, Nov. 2020.
[5] M. A. Bahmani and T. Thiringer, "Accurate evaluation of leakage inductance in high-frequency transformers using an improved frequency-dependent expression," *IEEE Trans. Power Electron.*, vol. 30, no. 10, pp. 5738–5745, Oct. 2015.
[6] M. Kharezy, M. Eslamian, and T. Thiringer, "Insulation design of a medium frequency power transformer for a cost-effective series high voltage DC collection network of an offshore wind farm," in *Proc. 21st Int. Symp. High Voltage Eng. (ISH)*, Budapest, Hungary, 2019, pp. 1406–1417.
[7] M. Kharezy, H. R. Mirzaei, Y. Serdyuk, T. Thiringer, and M. Eslamian, "A novel oil-immersed medium frequency transformer for offshore HVDC wind farms," *IEEE Trans. Power Del.*, early access, Nov. 3, 2020, doi: 10.1109/TPWRD.2020.3035718.
[8] M. A. Bahmani, T. Thiringer, A. Rabiei, and T. Abdulahovic, "Comparative study of a multi-MW high-power density DC transformer with an optimized high-frequency magnetics in all-DC offshore wind farm," *IEEE Trans. Power Del.*, vol. 31, no. 2, pp. 857–866, Apr. 2016.
[9] M. Mogorovic and D. Dujic, "Sensitivity analysis of medium-frequency transformer designs for solid-state transformers," *IEEE Trans. Power Electron.*, vol. 34, no. 9, pp. 8356–8367, Sep. 2019.
[10] G. Ortiz, J. Biela, and J. W. Kolar, "Optimized design of medium frequency transformers with high isolation requirements," in *Proc. 36th Annu. Conf. IEEE Ind. Electron. Soc. (IECON)*, Glendale, AZ, USA, Nov. 2010, pp. 631–638.
[11] Z. Ouyang, J. Zhang, and W. G. Hurley, "Calculation of leakage inductance for high-frequency transformers," *IEEE Trans. Power Electron.*, vol. 30, no. 10, pp. 5769–5775, Oct. 2015.
[12] K. Zhang, W. Chen, X. Cao, P. Pan, S. W. Azeem, G. Qiao, and F. Deng, "Accurate calculation and sensitivity analysis of leakage inductance of high-frequency transformer with Litz wire winding," *IEEE Trans. Power Electron.*, vol. 35, no. 4, pp. 3951–3962, Apr. 2020.
[13] A. Fouineau, M.-A. Raulet, B. Lefebvre, N. Burais, and F. Sixdenier, "Semi-analytical methods for calculation of leakage inductance and frequency-dependent resistance of windings in transformers," *IEEE Trans. Magn.*, vol. 54, no. 10, pp. 1–10, Oct. 2018.
[14] P. L. Dowell, "Effects of eddy currents in transformer windings," *Proc. Inst. Electr. Eng.*, vol. 113, no. 8, pp. 1387–1394, Aug. 1966.
[15] J. A. Ferreira, "Improved analytical modeling of conductive losses in magnetic components," *IEEE Trans. Power Electron.*, vol. 9, no. 1, pp. 127–131, Jan. 1994.
[16] M. Eslamian, M. Kharezy, and T. Thiringer, "An accurate analytical method for leakage inductance calculation of shell-type transformers with rectangular windings," *IEEE Access*, vol. 9, pp. 72647–72660, 2021, doi: 10.1109/ACCESS.2021.3080242.
[17] S. V. Kulkarni, S. A. Khaparde, *Transformer Engineering: Design, Technology, and Diagnostics*. New York, NY, USA: Taylor & Francis, 2013.
[18] K. Karsai, D. Kerényi, and L. Kiss, *Large Power Transformers*. Amsterdam, The Netherlands: Elsevier, 1987.
[19] R. M. Del Vecchio, B. Poulin, P. T. Feghali, D. M. Shah, and R. Ahuja, *Transformer Design Principles: With Applications to Core-Form Power Transformers*, 2nd ed. Boca Raton, FL, USA: CRC Press, 2010.
[20] X. Guo, C. Li, Z. Zheng, and Y. Li, "A general analytical model and optimization for leakage inductances of medium-frequency transformers," *IEEE J. Emerg. Sel. Topics Power Electron.*, early access, Feb. 24, 2021, doi: 10.1109/JESTPE.2021.3062019.
[21] A. Boyajian, "Leakage reactance of irregular distributions of transformer windings by the method of double Fourier series [includes discussion]," *Trans. Amer. Inst. Electr. Eng. III, Power App. Syst.*, vol. 73, no. 2, pp. 1078–1086, Jan. 1954.
[22] E. Roth, "Étude analytique du champ de fuites des transformateurs et des efforts mécaniques exercés sur les enroulements," *Revue Générale Del'électricité*, vol. 23, pp. 773–787, May 1928.
[23] A. L. Morris, "The influence of various factors upon the leakage reactance of transformers," *J. Inst. Electr. Eng.*, vol. 86, no. 521, pp. 485–495, May 1940, doi: 10.1049/jiee-1.1940.0068.
[24] E. Billig, "The calculation of the magnetic field of rectangular conductors in a closed slot, and its application to the reactance of transformer windings," *Proc. IEE IV, Inst. Monographs*, vol. 98, no. 1, pp. 55–64, Oct. 1951, doi: 10.1049/pi-4.1951.0007.
[25] P. Hammond, "Roth's method for the solution of boundary-value problems in electrical engineering," *Proc. Inst. Elect. Eng.*, vol. 114, no. 12, pp. 1969–1976, Dec. 1967.
[26] M. Eslamian, M. Kharezy, and T. Thiringer, "Calculation of the leakage inductance of medium frequency transformers with rectangular-shaped windings using an accurate analytical method," in *Proc. 21st Eur. Conf. Power Electron. Appl. (EPE ECCE Eur.)*, Genoa, Italy, Sep. 2019, pp. 3–5.
[27] M. Lambert, F. Sirois, M. Martinez-Duro, and J. Mahseredjian, "Analytical calculation of leakage inductance for low-frequency transformer modeling," *IEEE Trans. Power Del.*, vol. 28, no. 1, pp. 507–515, Jan. 2013.
[28] X. Margueron, A. Besri, P.-O. Jeannin, J.-P. Keradec, and G. Parent, "Complete analytical calculation of static leakage parameters: A step toward HF transformer optimization," *IEEE Trans. Ind. Appl.*, vol. 46, no. 3, pp. 1055–1063, May/Jun. 2010.
[29] I. Hernandez, F. de Leon, and P. Gomez, "Design formulas for the leakage inductance of toroidal distribution transformers," *IEEE Trans. Power Del.*, vol. 26, no. 4, pp. 2197–2204, Oct. 2011.
[30] R. Schlesinger and J. Biela, "Comparison of analytical models of transformer leakage inductance: Accuracy versus computational effort," *IEEE Trans. Power Electron.*, vol. 36, no. 1, pp. 146–156, Jan. 2021, doi: 10.1109/TPEL.2020.3001056.
[31] O. Andersen, "Transformer leakage flux program based on the finite element method," *IEEE Trans. Power App. Syst.*, vol. PAS-92, no. 2, pp. 682–689, Mar. 1973, doi: 10.1109/TPAS.1973.293773.
[32] P. Silvester and A. Konrad, "Analysis of transformer leakage phenomena by high-order finite elements," *IEEE Trans. Power App. Syst.*, vol. PAS-92, no. 6, pp. 1843–1855, Nov. 1973, doi: 10.1109/TPAS.1973.293564.

[33] M. Nazmunnahar, S. Simizu, P. R. Ohodnicki, S. Bhattacharya, and M. E. McHenry, "Finite-element analysis modeling of high-frequency single-phase transformers enabled by metal amorphous nanocomposites and calculation of leakage inductance for different winding topologies," *IEEE Trans. Magn.*, vol. 55, no. 7, pp. 1–11, Jul. 2019.
[34] L. Rabins, "Transformer reactance calculations with digital computers," *Trans. Amer. Inst. Elect. Eng. I, Commun. Electron.*, vol. 75, no. 3, pp. 261–267, 1956.
[35] M. Abramowitz and I. A. Stegun, *Handbook of Mathematical Functions*. New York, NY, USA: Dover, 1972.

MORTEZA ESLAMIAN received the M.Sc. and Ph.D. degrees in electrical engineering from Amirkabir University of Technology, Tehran, Iran, in 2009 and 2014, respectively. He has been a member of Iran Transformer Research Institute (ITRI), since 2005, where he has directed several industrial projects in the area of power transformers. Since 2014, he has been with the Department of Electrical Engineering, University of Zanjan, Iran, where he is currently an Assistant Professor. His research interests include power and special transformers, power system transients, high voltage and electrical insulation, and electrical installation and distribution systems.

MOHAMMAD KHAREZY (Member, IEEE) received the B.Sc. degree in electrical engineering from the University of Tabriz, in 1991, and the M.Sc. and Licentiate degrees in electrical engineering from Chalmers University of Technology, Sweden, in 2014 and 2020, respectively, where he is currently pursuing the Ph.D. degree in electrical power industrial. He worked for 18 years in the field of power transformers. Since 2011, he has been working as a High Voltage Researcher with the RISE Research Institutes of Sweden. He has contributed to several international scientific articles. His research interests include medium frequency power transformers, and high-voltage insulation, measurement, and testing technologies. He is a member of Cigré.

TORBJÖRN THIRINGER (Senior Member, IEEE) received the M.Sc. and Ph.D. degrees from Chalmers University of Technology, Gothenburg, Sweden, in 1989 and 1996, respectively. He currently works with Chalmers University of Technology, as a Professor in applied power electronics. His research interests include the modeling, control, and grid integration of wind energy converters into power grids, battery technology from detailed cell modeling to system aspects, and power electronics and drives for other types of applications, such as electrified vehicles, buildings, and industrial applications.